Coordinated Control of Active Devices to Alter Vehicle Rollover Tendencies

Allan Y. Lee
Jet Propulsion Laboratory
California Institute of Technology
M.S. 198-235, 4800 Oak Grove Drive, Pasadena, CA 91109-8099.

Summary

A Variable Dynamic Testbed Vehicle is presently being built for the National Highway Traffic Safety Administration. It will have four-wheel steering, front and rear active antiroll bar systems, four adjustable shock absorbers, and other active controls. Using these active systems, we can alter the vehicle's understeer coefficient, front/rear load transfer distribution in high-g lateral maneuvers, and roll mode frequency and damping. This study investigates how these active systems could be controlled to alter the vehicle rollover tendencies. In particular, we study how an increased front antiroll bar stiffness, in conjunction with an increased front damper rate and out-of-phase rear steering, could improve vehicle rollover resistance in high-g lateral maneuvers. Conversely, we also investigate how an increased rear antiroll bar stiffness, in conjunction with a decreased rear damper rate and in-phase rear steering, could degrade the vehicle's rollover resistance. Results obtained could provide guidelines for the safe operation of these controlled systems in limit lateral maneuvers.

Keywords: Active antiroll bar, adjustable dampers, four-wheel steering, load transfer distribution, rollover tendencies.

Introduction

To study the correlation between vehicle response characteristics and driver commands relative to crash avoidance, the National Highway Traffic Safety Administration's Office of Crash Avoidance Research (OCAR) has at its disposal a comprehensive set of tools and facilities. These include the Vehicle Research and Test Center and the (currently being built) National Advanced Driving Simulator. To augment these tools and facilities, a Variable Dynamics Testbed Vehicle (VDTV)[1] is presently being built for OCAR. This vehicle will be capable of emulating a broad range of automobile dynamic characteristics, allowing it to be used in crash avoidance systems development and in driving-related human factors research, among other areas. A similar but more limited experimental vehicle, called Variable Response Vehicle, was developed in the 1970s by the General Motors Corporation for vehicle handling research.[2] This vehicle has independent electrohydraulically controlled front and rear steering and steering force systems, enabling it to emulate a variety of vehicle directional control characteristics.

To emulate the dynamics of a broad range of vehicles, the steering, suspension, and braking subsystems of the VDTV must be "programmable." To accomplish this goal, the VDTV will have the following set of "active" elements: a four-wheel steering (4WS) system, both front and rear active antiroll bar controlled systems, and four continuously variable shock absorbers, among others. Software changes made to the algorithms that control these active subsystems can then effect significant changes in the vehi-
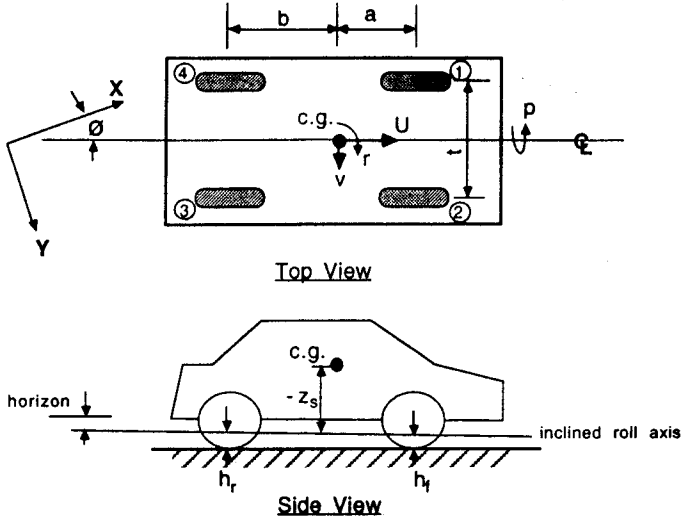
Top View

Side View

Figure 1: Schematic diagram of a passenger vehicle

cle's understeer coefficient, the front/rear load transfer distribution in lateral maneuvers, and the roll mode frequency and damping. This study investigates, via a nonlinear dynamic simulation program, how these active systems can be controlled to alter the vehicle rollover tendencies. In particular, we study how increasing the stiffness of the front antiroll bar, in conjunction with an increased front damper rate and out-of-phase rear steering, could improve vehicle rollover resistance in high-g lateral maneuvers. Conversely, we also investigate how an increased rear antiroll bar stiffness, in conjunction with a decreased rear damper rate and in-phase rear steering, could degrade the vehicle's rollover resistance.

Vehicle Dynamics Model

Consider a vehicle moving over a flat and level road surface (Fig. 1). When the forward speed, U, is kept constant, this vehicle model has three-degrees of freedom represented by the side velocity v, the roll rate p, and the yaw rate r. The side velocity v is defined at the point where the vehicle's inclined roll axis intersects a vertical plane that passed through the vehicle's center of gravity (c.g.). The side velocity is that component of the vehicle velocity vector that is perpendicular to the axis of symmetry of the vehicle. The cornering forces generated by the four tires are

denoted by F_{yi} ($i = 1$ to 4). The corresponding aligning torques generated at these tires are denoted by N_i ($i = 1$ to 4). Ignoring all contributions due to pitching dynamics, the equations of motion are:[3]

$$(I_{zz_s} + I_{zz_u})\dot{r} - (I_{xz_s} - I_{zz_u}\tan\triangle)\dot{p}$$
$$= a\cos\delta_f \sum_{i=1}^{2} F_{yi} - b\cos\delta_r \sum_{i=3}^{4} F_{yi}$$
$$+ \sum_{i=1}^{4} N_i + \frac{t}{2}\sin\delta_f(F_{y2} - F_{y1})$$
$$+ \frac{t}{2}\sin\delta_r(F_{y3} - F_{y4}), \tag{1}$$

$$(M_s + M_u)(Ur + \dot{v}) - M_s z_s \dot{p}$$
$$= \cos\delta_f \sum_{i=1}^{2} F_{yi} + \cos\delta_r \sum_{i=3}^{4} F_{yi}, \tag{2}$$

$$(I_{xx_s} + I_{xz_s}\tan\triangle)\dot{p} - (I_{xz_s} + I_{zz_s}\tan\triangle)\dot{r}$$
$$- M_s z_s(Ur + \dot{v}) = -(D_f + D_r)p$$
$$- (K_f + K_r + M_s g z_s)\phi, \tag{3}$$

$$\dot{\phi} = p, \tag{4}$$

where a and b define the location of the vehicle's c.g. between the axles, and M_s and I_{zz_s} denote the sprung mass and the yaw moment of inertia of the vehicle's sprung mass, respectively. Similarly, M_u and I_{zz_u} denote the unsprung mass and the yaw moment of inertia of the vehicle's unsprung mass, respectively. The roll moment of inertia of the sprung mass with respect to the roll axis is denoted by I_{xx_s} while I_{xz_s} denotes the roll-yaw product of inertias of the sprung mass. In (3,4), ϕ denotes the roll angle of the vehicle's sprung mass about the inclined roll axis, and $-z_s$ is the height of the sprung mass c.g. above the inclined roll axis. The slope of the inclined roll axis is $\tan\triangle = (h_f - h_r)/(a + b)$, where h_f and h_r denote the heights of the inclined roll axis above the ground plane at the front and rear axles, respectively. Estimated magnitudes of various vehicle parameters are given in Table 1.

In (3), the roll stiffness of the vehicle at the front and rear axles each contains two components. The first component represents that contributed by the passive suspension springs (K_{fP} and K_{rP}), and the second component is that

Table 1 Vehicle Parameter Values (with a driver and test equipment)

Vehicle Parameters	Values
sprung mass (kg)	1819
unsprung mass (kg)	200
wheel base (m)	2.69
track width (m)	1.55
c.g. distance to front axle (m)	1.02
c.g. height above ground (m)	0.538
front/rear height of roll axis above ground (m)	0.046 0.0066
sprung roll inertia (kg-m^2)	494
unsprung roll inertia (kg-m^2)	131
inertia about inclined roll axis (kg-m^2)	1072
yaw-roll product of inertias (kg-m^2)	0
sprung yaw inertia (kg-m^2)	2442
unsprung yaw inertia (kg-m^2)	475
front/rear roll camber coefficient (deg/deg)	0.741 0.894
front/rear roll steer coefficient (deg/deg)	0 0
front/rear roll stiffnesses (N-m/deg)	1186 798
front/rear roll damping (N-m-s/deg)	48.9 48.9
front/rear steering actuator bandwidth (Hz)	15 15
front/rear antiroll bar actuator bandwidth (Hz)	12 12

contributed by an active antiroll bar (K_{fA} and K_{rA}).

$$K_f \triangleq K_{fP} + K_{fA} \qquad (5)$$

$$K_r \triangleq K_{rP} + K_{rA} \qquad (6)$$

Since both K_{fA} and K_{rA} can be actively controlled, we can, in real time, alter the following load transfer distribution factor, κ_c:

$$\kappa_c \triangleq \frac{K_f - K_r}{K_f + K_r} \qquad (7)$$

To account for the actuator dynamics of the front and rear antiroll-bar systems, the instantaneous load transfer distribution factor, κ, is related to

κ_c by the following relation:

$$\tau_\phi \dot{\kappa} + \kappa = \kappa_c \qquad (8)$$

where τ_ϕ is the time constant of the active antiroll-bar system (cf. Table 1). Similarly, the front and rear damping coefficients in (3) can be actively controlled using four adjustable dampers. The instantaneous damping rates are:

$$D_f \triangleq \eta_f D_{fP} \qquad (9)$$

$$D_r \triangleq \eta_r D_{rP} \qquad (10)$$

where D_{fP} and D_{rP} represent the nominal passive damping rates at the vehicle's front and rear axles, respectively (cf. Table 1). The control variables, η_f and η_r, which vary between 0.5 and 2.5, are used to alter the vehicle roll mode damping.

The lateral force and aligning torque produced by a tire are both related to the tire slip angle and the normal loading on that tire. The commanded slip angles α_{fc} and α_{rc} at the front and rear axles are given respectively by the following kinematic relations:

$$\alpha_{fc} = \tan^{-1}\left(\frac{v + ar - h_f p}{U}\right) - \delta_f - E_{\phi f}\phi \qquad (11)$$

$$\alpha_{rc} = \tan^{-1}\left(\frac{v - br - h_r p}{U}\right) - \delta_r - E_{\phi r}\phi \qquad (12)$$

where δ_f and δ_r denote the front and rear steering angles, respectively. The parameters $E_{\phi f}$ and $E_{\phi r}$ are the roll steer coefficients at the front and rear axles, respectively. These commanded slip angles are related to the instantaneous slip angles via the following second-order dynamic relations:[4]

$$\ddot{\alpha}_f + 2\zeta\Omega\dot{\alpha}_f + \Omega^2\alpha_f = \Omega^2\alpha_{fc} \qquad (13)$$

$$\ddot{\alpha}_r + 2\zeta\Omega\dot{\alpha}_r + \Omega^2\alpha_r = \Omega^2\alpha_{rc} \qquad (14)$$

where ζ and Ω are the damping ratio and natural frequency of the second-order tire dynamics. The natural frequency can be estimated by: $\Omega = U/L_{\text{relax}}$, where L_{relax} is the relaxation length of the tire (cf. Table 2).

The normal loadings on the four tires are given by the following expressions:

$$F_{z1} = (M_s + M_u)\frac{bg}{2(a+b)} + \xi_f \qquad (15)$$

$$F_{z2} = (M_s + M_u)\frac{bg}{2(a+b)} - \xi_f \qquad (16)$$

$$F_{z3} = (M_s + M_u)\frac{ag}{2(a+b)} - \xi_r \qquad (17)$$

$$F_{z4} = (M_s + M_u)\frac{ag}{2(a+b)} + \xi_r \qquad (18)$$

where ξ_f and ξ_r denote the load transfers at the front and rear axles of the vehicle, respectively. These load transfers are proportional to the lateral acceleration a_y of the vehicle's sprung mass:

$$a_y = Ur + \dot{v} + (-z_s)\dot{p} \qquad (19)$$

$$\xi_f = (M_s + M_u)\frac{a_y(-z_s)}{2t}(1 + \kappa) \qquad (20)$$

$$\xi_r = (M_s + M_u)\frac{a_y(-z_s)}{2t}(1 - \kappa) \qquad (21)$$

where κ is the load transfer distribution factor, defined in (8), and t is the average track width of the vehicle. The expression for the lateral acceleration a_y is true only if $K_f + K_r \gg M_s(-z_s)g$ and $K_f(-z_s) \gg (K_f + K_r)b/(a + b)h_f$. These inequality conditions are satisfied in our study.

In arriving at (11,12), we have assumed that the vehicle has both front and rear steering actuators. In our study, first-order models are used to account for both the front and rear steering actuator dynamics:

$$\tau_f \dot{\delta}_f + \delta_f = \delta_{fc} \qquad (22)$$

$$\tau_r \dot{\delta}_r + \delta_r = \delta_{rc} \qquad (23)$$

Here δ_{fc} and δ_{rc} are commands to the front and rear steering actuators, respectively. In (22-23), τ_f and τ_r are the time constants of the front and rear steering actuators, respectively (cf. Table 1).

Kinematic Model

In addition to the above described dynamic equations, the following kinematic relations are used to compute the resultant vehicle heading and trajectory:

$$\dot{\psi} = r \qquad (24)$$

$$\dot{x} = U\cos\psi - v\sin\psi \qquad (25)$$

$$\dot{y} = U\sin\psi + v\cos\psi \qquad (26)$$

In Fig. 1, x and y are the rectilinear coordinates of the vehicle's c.g. relative to an arbitrary reference origin. The angle ψ is the angle formed between the vehicle's longitudinal axis and the x axis, defined to be positive in the clockwise direction.

Tire Model

A nonlinear tire model documented in Ref. 5 is used in this study. When the tire's slip ratio is zero, we have the following simplified expressions that relate the tire's lateral force and aligning torque to its slip angle, camber angle, and normal loading.

Composite slip

$$\sigma_i = \text{sgn}(\alpha_i)\frac{\pi\tan\alpha_i}{4F_{zi}\mu_i}(A_0 + A_1 F_{zi} - \frac{A_1}{A_2}F_{zi}^2) \quad (27)$$

for $i = 1$ to 4, and μ_i is the coefficient of friction between the ith tire and the road surface. The normal loadings F_{zi} were given in (15-18), while the tire slip angle α_i was defined in (13-14). Note that $\alpha_1 = \alpha_2 = \alpha_f$ and $\alpha_3 = \alpha_4 = \alpha_r$. The parameters A_j ($j = 0, 1$, and 2) are Calspan coefficients that were determined experimentally. Magnitudes of these and other Calspan tire coefficients are given in Table 2.

Road/tire coefficient of friction

$$\mu_i = \overbrace{(B_1 F_{zi} + B_3 + B_4 F_{zi}^2)}^{\text{peak friction coefficient at } i^{th} \text{ tire}}\frac{N_{\text{simulation}}}{N_{\text{test}}}$$
$$\times \{1 - K_\mu \text{ sgn}(\alpha_i)\sin\alpha_i\} \qquad (28)$$

for $i = 1$ to 4, and $N_{\text{simulation}}$ and N_{test} are the skid numbers of the road surface used in this simulation study and the test surface on which another set of Calspan coefficients, B_j ($j = 1, 3$, and 4), were determined. The Calspan parameter K_μ is also determined experimentally.

Tire force saturation function

$$f(\sigma_i) = \frac{C_1\sigma_i^3 + C_2\sigma_i^2 + \frac{4}{\pi}\sigma_i}{C_1\sigma_i^3 + C_3\sigma_i^2 + C_4\sigma_i + 1} \qquad (29)$$

for $i = 1$ to 4, and the tire saturation coefficients C_j ($j = 1$ to 4) were obtained via curve fittings of test data.

Camber thrust

$$F_{\gamma i} = (A_3 F_{zi} - \frac{A_3}{A_4}F_{zi}^2)\gamma_i\{1 - K_\gamma f^2(\sigma_i)\} \quad (30)$$

for $i = 1$ to 4, and γ_i is the camber angle of the ith tire. Note that $\gamma_1 = \gamma_2 = \gamma_f$, and $\gamma_3 = \gamma_4 = \gamma_r$. The parameters K_γ and A_j ($j = 3$ and

4) are Calspan coefficients that were determined experimentally.

Normalized side force

$$\frac{F_{yi}}{\mu_i F_{zi}} = -\text{sgn}(\alpha_i) f(\sigma_i) + \frac{F_{\gamma i}}{\mu_i F_{zi}} \quad (31)$$

for $i = 1$ to 4, and μ_i and $f(\sigma_i)$ were defined in (28) and (29), respectively. The normal loadings F_{zi} were given in (15-18), and the camber thrust $F_{\gamma i}$ was given in (30). The lateral force generated by the ith tire, F_{yi}, was used in (1-2).

Aligning torque

$$N_i = -\frac{K_1 F_{zi} \tan \alpha_i}{(1 + G_1 \sigma_i^2)^2} (A_0 + A_1 F_{zi} - \frac{A_1}{A_2} F_{zi}^2) \quad (32)$$

for $i = 1$ to 4, and the parameters K_1 and G_1 are Calspan coefficients that are determined experimentally. The aligning torque generated by the ith tire, N_i, was used in (1).

Table 2 Calspan Tire Coefficients (P205/75R15)
{British units were used in Ref. 6}

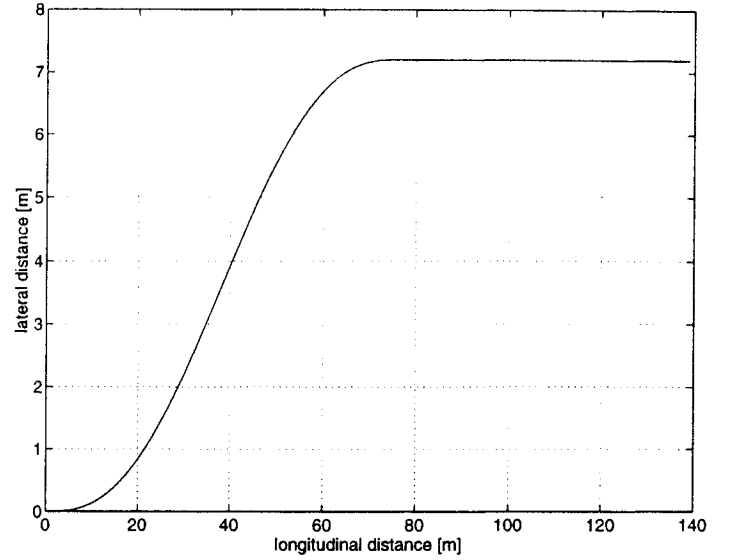| Calspan Coefficients	Estimated Values
A_0 (lb.wt./rad)	5000
A_1 (rad^{-1})	6.40
A_2 (lb.wt./rad)	3700
A_3 (rad^{-1})	0.353
A_4 (lb.wt.)	-2630
B_1 (lb.wt.$^{-1}$)	-0.000135
B_3 (-)	1.09
B_4 (lb.wt.$^{-2}$)	1.0e-8
C_1 (-)	1.00
C_2 (-)	0.34
C_3 (-)	0.57
C_4 (-)	0.32
K_μ (-)	0.234
K_γ (-)	0.90
L_{relax} (ft)	1.0
ζ (-)	0.8
$N_{\text{simulation}}$	0.92
N_{test}	0.85
K_1 (ft/lb.wt.)	-0.000215
G_1 (-)	1.0

Figure 2: A reference two-lane change trajectory

High-g Two-Lane Change Maneuvers

A severe two-lane change maneuver typically involves a large two-way load transfer between the inside and outside tires. In extreme cases, it can lead to the lifting of one or more tires above ground, resulting in a rollover.[6] In our study, we use the following fifth-order polynomial to represent the desired lane change trajectory that the driver would like to track closely:[7]

$$y_r(x) = y_f \{10(\frac{x}{x_f})^3 - 15(\frac{x}{x_f})^4 + 6(\frac{x}{x_f})^5\} \quad (33)$$

where x_f and y_f denote the position of the vehicle at the end of the lane change. In our two-lane change maneuver, $y_f = D$ and $x_f = U \times T_{lc}$, where T_{lc} is the lane change time. Fig. 2 illustrates this fifth-order trajectory for the following nominal scenario: $U = 125$ km/h, $D = 7.2$ m, and $T_{lc} = 2.2$ s. From (33) we can compute the reference curvature c_r and reference heading angle ψ_r of this trajectory:

$$\frac{dy}{dx}(x) = 30x^2(x_f - x)^2 y_f / x_f^5 \quad (34)$$

$$\frac{d^2 y}{dx^2}(x) = 60x y_f (x_f - x)(x_f - 2x)/x_f^5 \quad (35)$$

$$\psi_r(x) = \tan^{-1}(\frac{dy}{dx}) \quad (36)$$

$$c_r(x) = \frac{d^2 y}{dx^2} / \{1 + (\frac{dy}{dx})^2\}^{\frac{3}{2}} \quad (37)$$
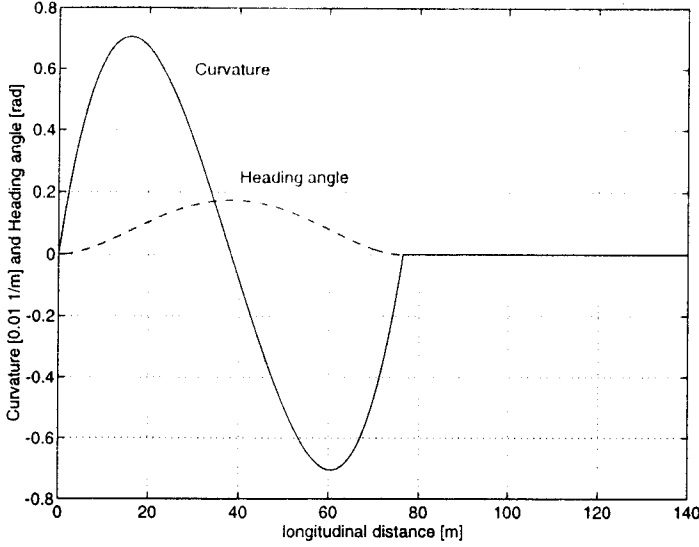
Figure 3: Reference curvature and heading angle of a two-lane change trajectory

The variations of the reference heading and curvature with the longitudinal distance are illustrated in Fig. 3.

To track this trajectory, a driver uses a combined feedforward and feedback control law to steer the vehicle. Let us define:

$$\Delta\psi(t) = \psi_r(t) - \psi(t) \qquad (38)$$

$$\Delta y(t) = y_r(t) - y(t) \qquad (39)$$

$$\Delta c(t) = c_r(t) - r/U \qquad (40)$$

$$\delta_{fc}(t) = \overbrace{K_c c_r(t + t_p)}^{\text{feedforward}} + \underbrace{K_{\Delta c}\Delta c(t) + K_{\Delta\psi}\{\Delta\psi(t) + K_{\Delta y}\Delta y(t)\}}_{\text{feedback}} \qquad (41)$$

Here, $c_r(t + t_p)$ is the reference curvature at a look-ahead distance as determined by the driver's preview time t_p. Curvature deviation $\Delta c(t)$ denotes the difference between the reference curvature and the current curvature of the vehicle, r/U. $\Delta y(t)$ denotes how far the vehicle's c.g. has deviated from the centerline of the reference trajectory, while $\Delta\psi(t)$ denotes how much the vehicle's axis of symmetry has deviated from the local tangent of the reference trajectory. The steering command is $\delta_{fc}(t)$. The feedforward gain is K_c and the feedback gains are $K_{\Delta c}$, $K_{\Delta y}$ and $K_{\Delta\psi}$. As conjectured in Ref. 8, we assume in this study that an experienced driver does not use the positional and heading errors to generate the steering command during the reflexive phase of the lane change maneuver. Instead, he executes an "open-loop" steering command based upon the estimated roadway curvature and his learnt knowledge of the vehicle's lateral characteristics. In the subsequent regulatory phase of the lane change maneuver, the driver will use small steering adjustments to zero out residuals in the vehicle's yaw rate, side velocity, heading angle, etc., in a "closed loop."

Vehicle Performance: Passive Vehicle

Using Eq. (41), we can compute the steering command needed to make a two-lane change maneuver. Time histories of the resultant passive vehicle responses are depicted in Figs. 4–11. These results were obtained for a two-lane change maneuver made with $U = 125$ km/h, $D = 7.2$ m, and $T_{lc} = 2.2$ s. Driver's model parameters used in this lane change are: $t_p = 0.13$ s, $K_c = 12.75$ rad-m, and $K_{\Delta c} = 2.45$ rad-m. This set of results will be used as a baseline to which results obtained using an actively controlled VDTV are compared with.

Figs. 4-7 depict the time histories of the vehicle's yaw rate, lateral acceleration, front steering angle, and roll angle, respectively. Figs. 8-11 depict the transient variations of the normal loadings at the four tires. In these figures, results obtained for the passive vehicle and the VDTV are plotted with solid and dashed lines, respectively. Details on how the VDTV results were obtained will be given in the next section.

For the vehicle used in our study, the static loadings on the rear tires are lower than those on the front tires. As such, in a high-g maneuver, the lowest tire loading will likely to occur at one of the two rear tires. To avoid a rollover, none of these tire loadings should be near zero. From Fig. 9 we observe that minimum loading on the left rear tire occurred at about the same time that the lateral acceleration peaks in the negative direction. This minimum tire loading, about 186 kg.wt., is also the lowest tire loading among all the tires throughout the lane change maneuver. Hence, there is no incipient rollover in this
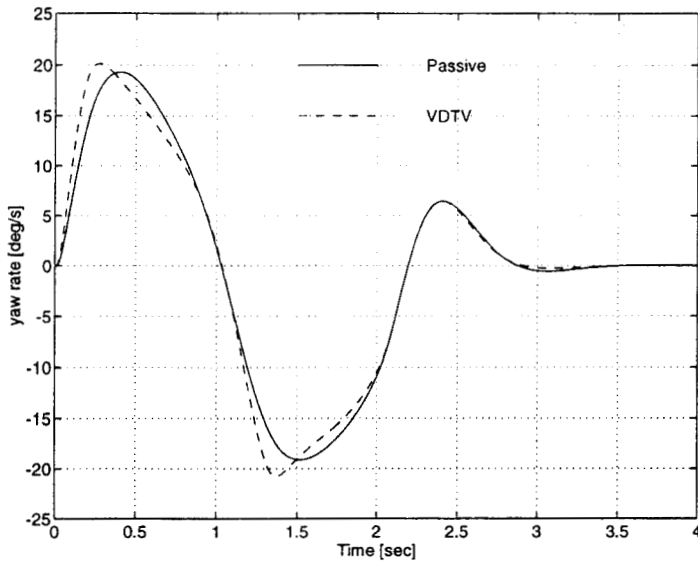
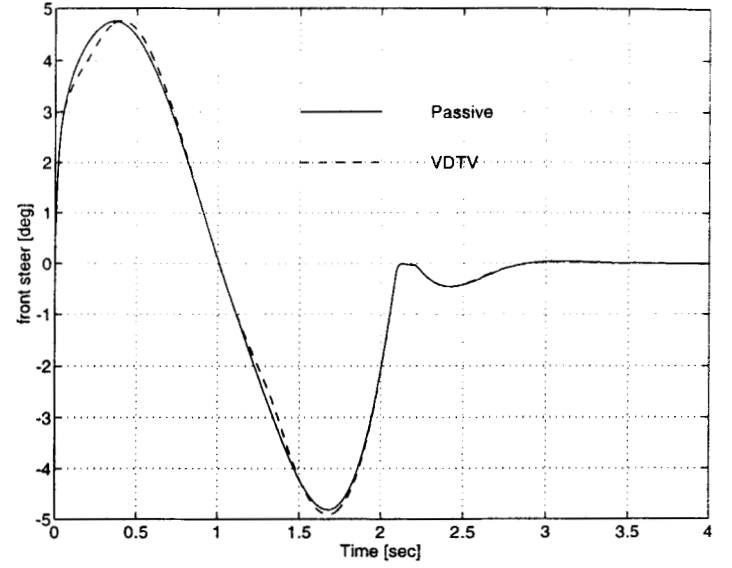Figure 4: Yaw rate responses of VDTV and passive vehicle

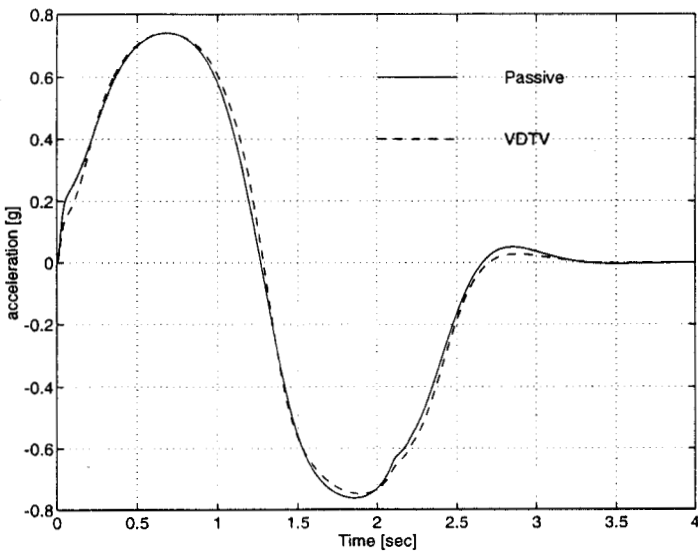Figure 6: Front steer angle of VDTV and passive vehicle

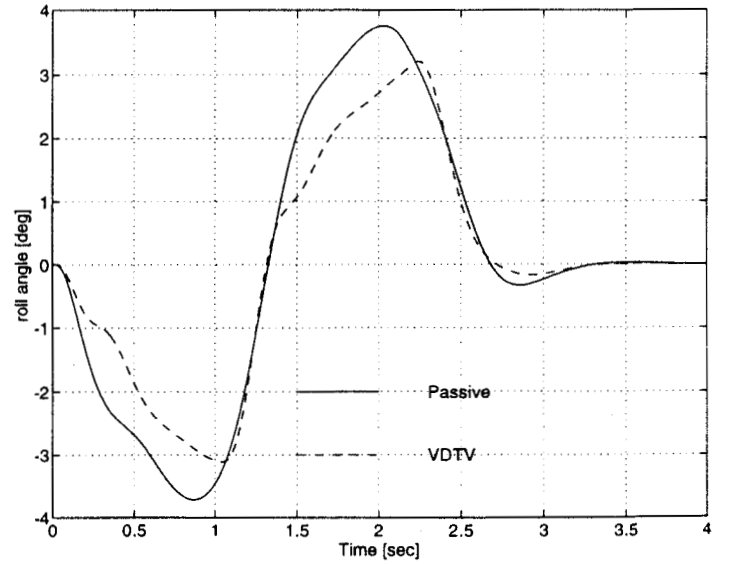Figure 5: Acceleration of VDTV and passive vehicle
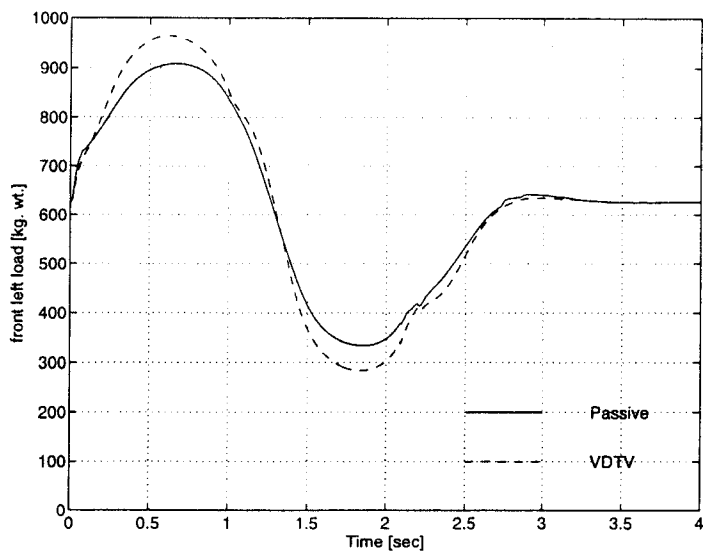

Figure 7: Roll angle of VDTV and passive vehicle

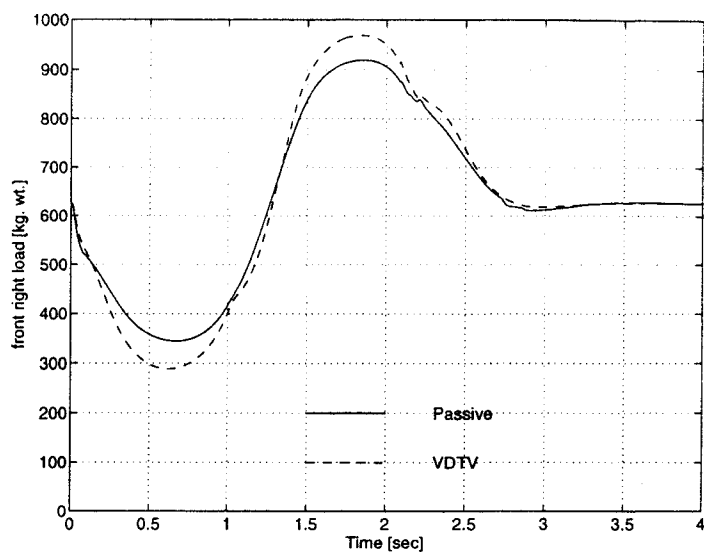Figure 8: Left front vehicle loadings
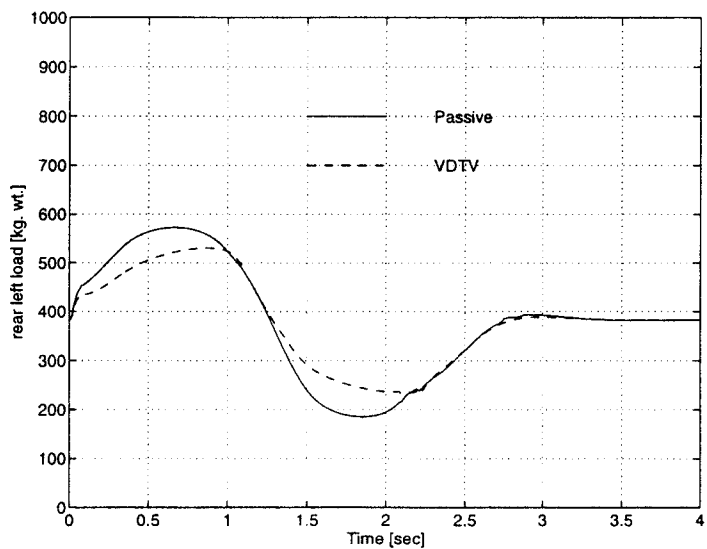
Figure 10: Right front vehicle loadings
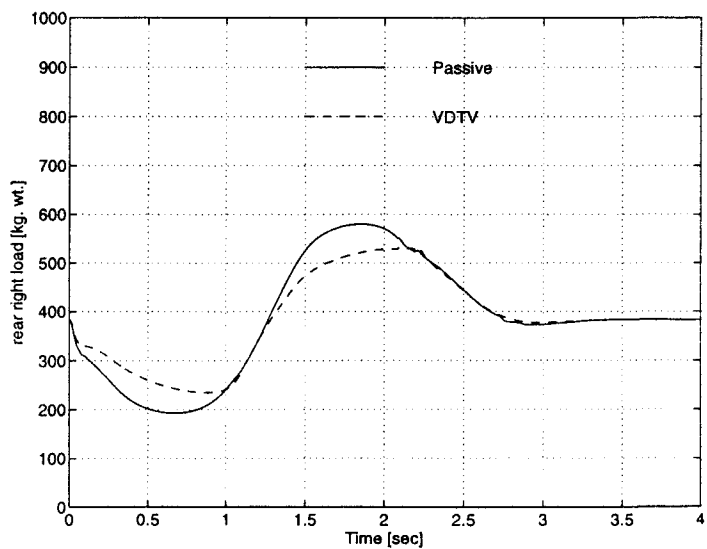
Figure 9: Left rear vehicle loadings

Figure 11: Right rear vehicle loadings

particular lane change maneuver. This is to be expected since the $t/(2h_{cg})$ ratio of the vehicle, about 1.45, is among the highest of all production vehicles. To get closer to a rollover, hard braking should be applied at the time when the vehicle roll angle is at a local maximum. This is to be followed immediately by a full brake release.[10] These braking commands affect the longitudinal dynamics of the vehicle, and is beyond the scope of the study.

Rollover resistance: How to improve it?

To increase the vehicle resistance to rollover, we can increase the stiffness of the active front antiroll bar K_{fA} with the vehicle yaw rate r: $K_{fA} \propto | r |$. The rationale for this control algorithm is as follows. The vehicle's lateral acceleration is related to the vehicle's yaw rate. If we increase the vehicle's front antiroll bar stiffness in a high-g maneuver, a larger proportion of the load transfer will be carried by the front axle, and that at the rear axle will be reduced. That being the case, the magnitude of the minimum loading on the rear left tire will increase, and the vehicle rollover resistance is improved. Alternative control algorithms that could achieve the same effect include: $K_{fA} \propto | \delta_{fc} |$, $K_{fA} \propto | a_y |$, $K_{fA} \propto a_y^2$, etc. See also Ref. 9. For brevity, only results obtained using the vehicle's yaw rate will be given in the following.

It is unlikely that a vehicle will rollover in a low-g maneuver. Hence, there is no motivation to activate the front active antiroll bar in these low-g scenarios. On the other hand, there is a mechanical limit to which the front antiroll-bar stiffness can approach. Considering these factors, the above suggested control algorithm is modified as follows:

$$K_{fA}^c = \begin{cases} 0 & \text{if } | r | \leq r_{db} \\ k_r | r - \text{sgn}(r)r_{db} | & \text{otherwise} \end{cases} \quad (42)$$

$$K_{fA} = \min\{K_{fA}^{\text{mech}}, K_{fA}^c\} \quad (43)$$

Here, K_{fA}^{mech} denotes the mechanical limit of the front antiroll bar stiffness, and r_{db} denotes a yaw rate deadband. If the vehicle yaw rate falls within $\pm r_{db}$, the front antiroll-bar control system will not be activated.

In this study, we select r_{db} to be 1.25 deg/sec which corresponds to a lateral acceleration of about 0.25 g (for the passive vehicle). The feedback gain k_r was selected as follows: Let us assume that our objective is to increase the minimum tire loading (at the left rear tire) from 186 to 240 kg.wt. in a 0.75-g lateral maneuver. The required value of κ that can accomplish this goal could be determined using equations (17) and (21). For $a_y = 0.75g$ and $F_{z3} = 240$ kg.wt., we have $\kappa = 0.462$. From equations (5-7), it is clear that a κ_c of 0.462 could be achieved if we have $K_{fA} = 984.2$ Nm/deg and $K_{rA} = 0$ Nm/deg (i.e., without using the rear anti-roll bar actuator). The peak value of the vehicle's yaw rate for a 0.75-g maneuver is about 20 deg/sec. Hence, the value of k_r should be $984.2/(20\text{-}1.25) \times 57.3^2 \approx 172{,}340$ Nm/rad per rad/s. This feedback gain is rounded to 200,000 Nm/rad per rad/s is this study. The magnitude of K_{fA}^{mech} is assumed to be identical to K_{fP}.

The increased front antiroll bar stiffness will cause the damping ratio of the vehicle roll motion to drop. To maintain the same roll damping ratio, the front damper rates must be increased by a factor that is proportional to the square root of the passive-to-active front roll stiffness ratio. The same is true for the rear axle. Thus, the adjustable dampers at the front and rear axles are controlled according to the following algorithms:

$$\eta_f = \sqrt{\frac{K_f}{K_{fP}}} \quad (44)$$

$$\eta_r = \sqrt{\frac{K_r}{K_{rP}}} \quad (45)$$

where η_f and η_r are the damping rate ratios defined in (9,10).

The time histories of the front steering command and the load transfer distribution factor obtained using control algorithms (42-45) are given in Figs. 12 and 13, respectively. Relative to the steering command used by the passive vehicle (cf. Fig. 6), that given in Fig. 12 is significantly larger. This is not unexpected because a vehicle's understeer coefficient typically increases with an increase in the front antiroll bar stiffness.[1] Hence, a larger steering angle must be used to achieve the same level of lateral acceleration ($\approx \pm 0.75$ g).
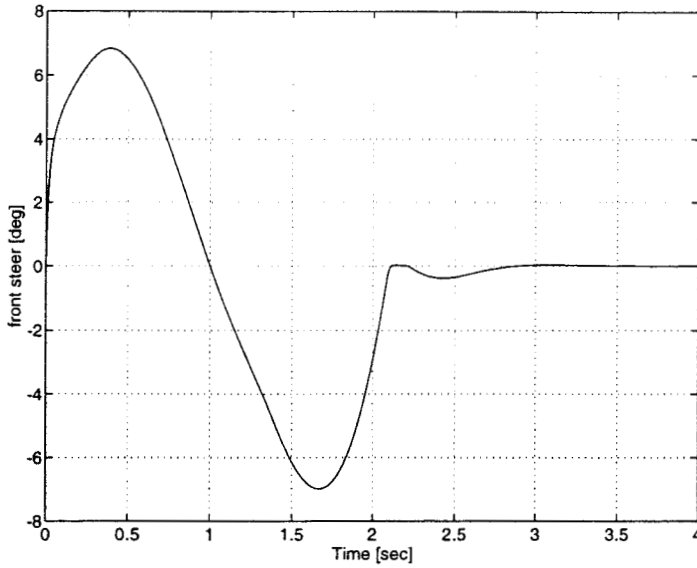
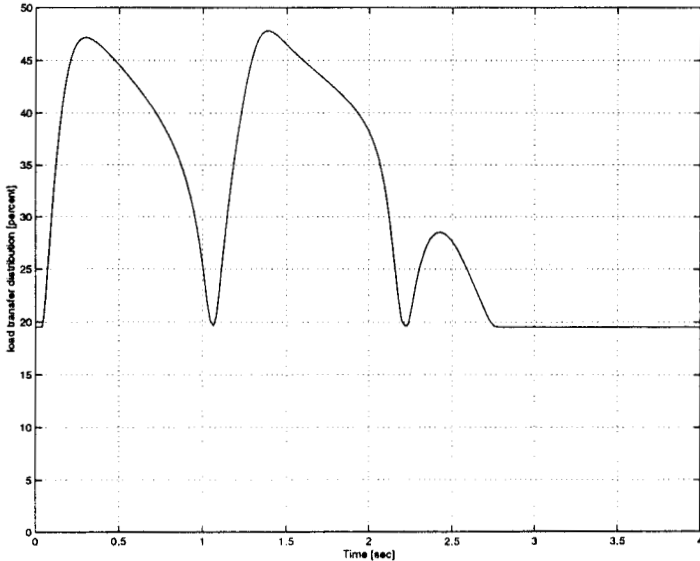Figure 12: Front steering angle of VDTV

Figure 13: Load transfer distribution factor of VDTV

Fig. 13 depicts the time history of the load transfer distribution factor κ. The "static" value of κ is about +20%. This means that the front and rear axles carry about 60% and 40%, respectively, of the total load transferred in a lateral maneuver (κ is the difference between 60% and 40%). With the front antiroll bar activated, the peak value of κ is near 48% (k_r was selected to achieve a κ of 46.2% when the lateral acceleration is ≈ 0.75g). That is, the front and rear axles, at the time when κ peaked, carry 74% and 26%, respectively, of the total load transfer. The reduced load transfer at the rear axle causes the minimum loading at the left rear tire to increase from 186 kg. wt. (for the passive vehicle) to 240 kg. wt. In this way the vehicle rollover resistance is improved. Not shown in Fig. 14 is the fact that the peak value of $K_{fA}/K_{fP} = 0.91$, and the mechanical limit of K_{fA} was never exceeded.

We can use the VDTV's 4WS system to overcome problems associated with the increased vehicle understeer coefficient. In particular, out-of-phase steering of the rear wheel typically produces an oversteer effect that can be used to cancel the understeer effect produced by the increased front antiroll bar stiffness. That is, whenever the front antiroll bar system is activated, we will simultaneously steer the rear wheels accordingly to the following relation: $\delta_{rc} = R \times \delta_{fc}$ Here, R denotes the front-to-rear wheel angle ratio, which is defined positive if the wheels are steered in phase. In this study, we use a ratio of −0.35 to produce an oversteer effect. Results obtained are given in Figs. 4-11 and 14.

As depicted in Fig. 4, the front steering angle command of the 4WS VDTV is almost identical to that used by the passive vehicle. The peak roll angle of the 4WS VDTV is smaller than that obtained with the passive vehicle (cf. Fig. 7) because of the increased front antiroll bar stiffness. The load transfer distribution ratio of the 4WS VDTV, depicted in Fig. 14, is about the same as that shown in Fig. 13. But it now peaks at a slightly higher value of 50% (instead of the 48% shown in Fig. 13).

Comparisons between the tire loadings of the passive vehicle and those of the 4WS VDTV are
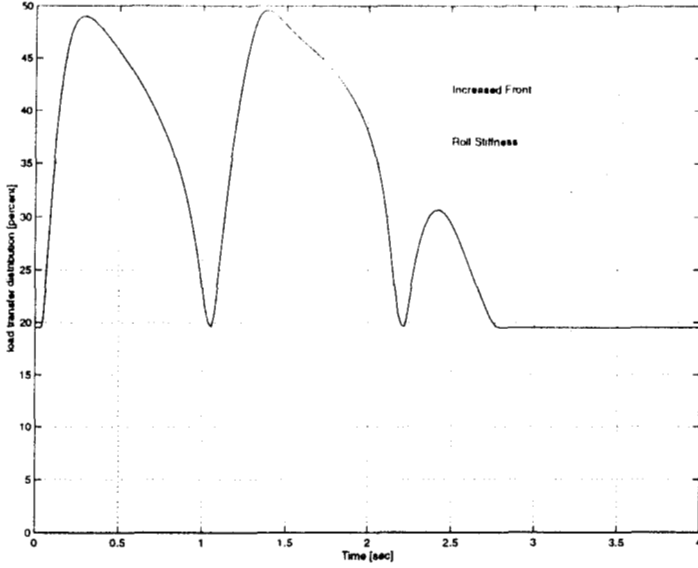
Figure 14: Load transfer distribution factor of the 4WS VDTV

Figure 15: Load transfer distribution factor of VDTV

given in Figs. 8-11. Since the front roll stiffness of the VDTV is larger than that of the passive vehicle, a larger proportion of the lateral load transfer is being carried at the VDTV's front axle. This is clearly reflected in the time histories of the two front tire loadings (the peak-to-peak of the dashed lines are larger than those of the solid lines). Also, with smaller load variations at the rear tires of the 4WS VDTV, its minimum tire loading is now larger than that of the passive vehicle. Thus, the rollover resistance of the VDTV is improved.

Rollover resistance: How to lower it?

To study accidents involving a vehicle rollover, there might be a need to artificially lower the rollover resistance of a test vehicle. To this end, we might want to increase the roll stiffness of the *rear* antiroll bar:

$$K_{rA}^c = \begin{cases} 0 & \text{if } |r| \le r_{db} \\ k_r |r - \text{sgn}(r)r_{db}| & \text{otherwise} \end{cases} \quad (46)$$

$$K_{rA} = \min\{K_{rA}^{\text{mech}}, K_{rA}^c\} \quad (47)$$

Here, K_{rA}^{mech} denotes the mechanical limit of the rear antiroll bar stiffness, and r_{db} denotes a yaw rate deadband. The results given in the following were obtained with $r_{db} = 1.25$ deg/s, but it needs not be identical to that used in (42-43). The feedback gain k_r was selected as follows: Let
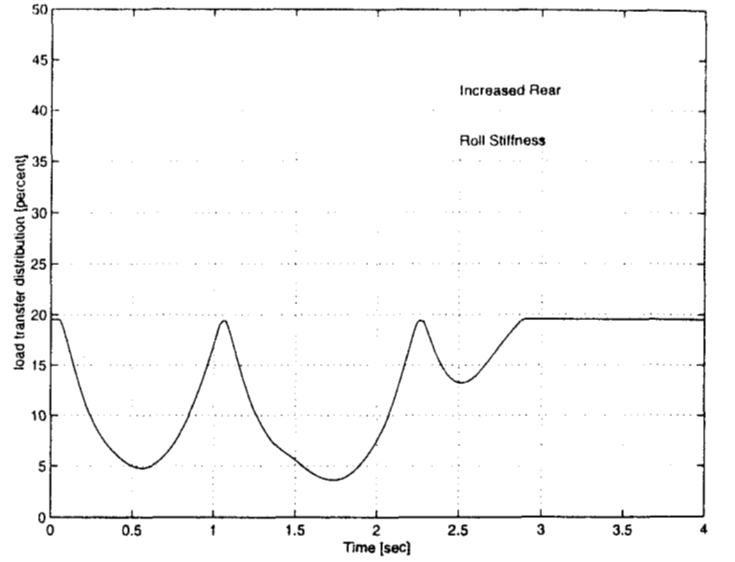
us assume that our objective is to reduce the minimum tire loading (at the left rear tire) from 186 to 140 kg.wt. in a 0.75-g lateral maneuver. The required value of κ determined using equations (17) and (21) is 0.08. From equations (5-7), it is clear that a κ_c of 0.08 could be achieved if we have $K_{fA} = 0$ Nm/deg (i.e., without using the front anti-roll bar actuator) and $K_{rA} = 212.3$ Nm/deg. The peak value of the vehicle's yaw rate for a 0.75-g maneuver is about 20 deg/sec. Hence, the value of k_r should be $212.3/(20-1.25) \times 57.3^2 \approx 37,200$ Nm/rad per rad/s. This feedback gain is rounded to 50,000 Nm/rad per rad/s is this study. The magnitude of K_{rA}^{mech} is assumed to be identical to K_{rP}.

Whenever the rear antiroll bar roll stiffness is increased, there will be a corresponding decrease in the vehicle understeer coefficient. To restore the understeer coefficient, we will steer the rear wheels in phase with the front wheels. That is, whenever the rear antiroll bar system is activated, we will simultaneously steer the rear wheels as follows: $\delta_{rc} = R \times \delta_{fc}$. In this study, we use a ratio of $+0.10$ to produce the required understeer effect. Results obtained are given in Figs. 15-16.

Fig. 15 depicts the time variation of the load transfer distribution factor κ. Here, we note that stiffening the rear antiroll bar system causes κ to
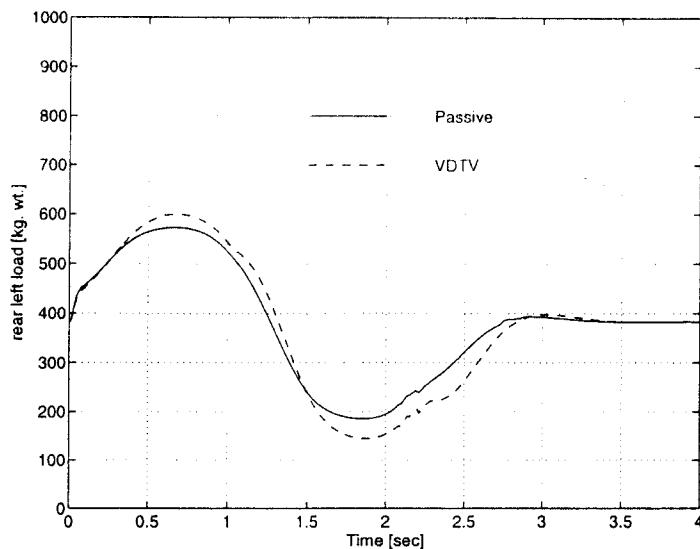
Figure 16: Left rear loadings of VDTV and passive vehicles

drop to as low as 4% (k_r was steered to achieve a κ of 8% when the lateral acceleration is about 0.75g). That is, the front and rear axles, at the time when κ is at a local minimum, carry 52% and 48%, respectively, of the total load transfer. The larger load transfer at the rear axle causes the minimum loading at the rear left tire to drop from 186 kg. wt. (for the passive vehicle) to 140 kg. wt. (see Fig. 16). In this way, the vehicle rollover resistance is degraded.

As an extreme scenario, consider the case when we would like to achieve a minimum tire loading of 100 kg.wt. The required value of κ is -0.072. To achieve a κ_c of -0.072, we could use a $K_{fA} = 0$ Nm/deg and $K_{rA} = 572.0$ Nm/deg. The magnitude of K_{rA} selected might be unnecessarily large. As an alternative, we could achieve the same κ_c using a $K_{fA} = -265.43$ Nm/deg and a $K_{rA} = +265.43$ Nm/deg. Note the use of a negative front antiroll bar stiffness. For brevity, results obtained using these combination of front and rear antiroll bar stiffnessese are not given here.

Summary
The Variable Dynamic Testbed Vehicle, currently being built for the National Highway Traffic Safety Administration will have four-wheel steering, front and rear active antiroll bar systems, and other active controls. Coordinated controls of these active devices could be made to singularly alter the vehicle front/rear load transfer distribution factor without affecting other vehicle characteristics such as its understeer coefficient. Candidate control algorithms that could alter the load distribution (and hence the vehicle's rollover resistance) are described in this study.

References

1. Lee, A., Marriott, A., and Le, N., "Variable Dynamic Testbed Vehicle: Dynamics Analyses," SAE 970560, 1997.

2. McKenna, K., "A variable response vehicle - description and applications," Joint Automatic Control Conference, Austin, Texas, June 1974.

3. Nordeen, D., "Vehicle directional control equations for an inclined roll axis," General Motors Proving Ground, Report No. A-2165, July 69.

4. Heydinger, G., Garrott, W., and Chrstos, J., "The importance of tire lag on simulated transient vehicle response," SAE 910235, 1991.

5. Allen, W., Magdaleno, R., Rosenthal, T., Klyde, D., and Hogue, J., "Tire model requirements for vehicle dynamics simulation," SAE 950312, 1995.

6. Allen, W., Szostak, H., Klyde, D., Rosenthal, T., and Owens, K., "Vehicle dynamic stability and rollover," DOT HS 807 956, Final Report, June 1992.

7. Nelson, W., "Continuous curvature path for autonomous vehicles," IEEE International Conference on Robotics and Automation, May 1989.

8. Lee, A., "Performance of four-wheel-steering vehicles in lane change maneuvers," SAE 950316, 1995.

9. Williams, D., and Haddad, W., "Nonlinear control of roll moment distribution to influence vehicle yaw characteristics," IEEE

Transactions on Control Systems Technology, Vol. 3, No. 1, March 1995.

10. Fancer, P.S., Erwin, D., Grote, P., et al, "Limit handling performance as influenced by degradation of steering and suspension systems," Vol. 1 of 2, DOT-HS-031-1-126, UM-HSRI-PF-72-3-1, November 1972.

Acknowledgments

Disclaimer

The discussion presented in this paper reflects the opinion and findings of the author, and not necessarily those of the National Highway Traffic Safety Adminstration.